International Journal of Theoretical Physics, Vol. 46, No. 6, June 2007 (© 2007)
DOI: 10.1007/s10773-006-9295-9

Semi-Analytical Solution of Dirac Equation in Schwarzschild-de Sitter Spacetime

Y. Lyu[1,3] and Y.-X. Gui[2]

Received August 19, 2006; accepted October 12, 2006
Published Online: January 23, 2007

In the present paper, we solve the radial parts of Dirac equation between the inner and the outer horizon in the Schwarzschild-de Sitter (SdS for short) geometry. Complete physical parameter space is divided into two regions depending on the height of the potential barrier and the energy of the incoming particle. In each region, we concentrate on two limiting cases. The first case is when the two horizons are close to each other and the second case is when the horizons are far apart. In each case, we give the semi-analytical solution by using WKB (Wentzel-Krames-Brillouin) approximation and show the instantaneous reflection and transmission coefficients as well as the radial wave functions graphically.

KEY WORDS: Dirac equation; Schwarzschild-de Sitter space.
PACS: 04.20.-q, 04.70.-s, 04.70.Dy, 95.30.Sf

1. INTRODUCTION

The curved spacetime outside a black hole is studied by many authors. Kinnersley (1969) introduced a null-tetrad frame in 1969. Teukolsky (1973) decoupled and separated the equations for gravitational, electromagnetic and neutrino field by using this null-tetrad frame. Chandrasekhar (1976); Chankrasekhar (1983) also used this null-tetrad frame to separate the Dirac equation in Kerr geometry into radial and angular parts. Then Page (1976) extended this work to Kerr–Newman geometry. Basing on the above work, Khanal discussed the problem about the reflection and transmission coeffients of the particles scattering from a black hole (Khanal and Panchapakesan, 1980; Khanal, 1984). Liu *et al.* (1980); Zhao *et al.* (1981) studied Hawking radiation of Dirac particles around semiextreme Kerr

[1] College of Physics and Technology, Shenyang Normal University, Shenyang 110034, Liaoning Province, P.R. China.
[2] Department of Physics, Dalian University of Technology, Dalian 116024, Liaoning Province, P.R. China.
[3] To whom correspondece should be addressed at College of Physics and Technology, Shenyang Normal University, Shenyang 110034, Liaoning Province, P.R. China; e-mail: yanlvthp@yahoo.com.cn.

and semi-extreme Kerr–Newman black hole separately. They only gave the solutions in the limiting case close to the horizon(s). While little work has been done to study the transimission properties in the whole range of the space. After Chakrabarti (1984) had solved the angular part of the Dirac equation in Kerr geometry and found the corresponding eigenvalues for different Kerr parameters, Mukhopadhyay and Chakrabarti (1999, 2000) solved the spatially complete radial equations in Schwarzschild and Kerr geometry, they calculated the local values of the reflection and transmission coefficients and gave analytical expressions of radial wave functions by using WKB approximation. Most prior works in this area have been concerned with the background spacetime without cosmological constant Λ. The spacetime with cosmological constant Λ is much less studied. One example is the study of Brevik and Simonsen (2001) about the scalar field equation in SdS space.

In the present paper, we solve the Dirac equation in SdS geometry. We consider the case that the particles scatter from the SdS black hole. This space is bounded by two horizons, an inner "black hole" horizon and an outer "cosmological" horizon, the latter being detemined by the cosmological constant Λ. What we are interested in is the region between the two horizons.

In the next section, we start by presenting the basic equation in SdS space. Then following Mukhopadhyay and Chakrabarti (1999, 2000), we also classify the parameter space in terms of physical and unphysical region and solve the wave equation in physical region. We consider two cases, one is when the two horizons are lying close to each other (being called Nariai case), the other is when the two horizons are wide separated. In Section 4 we give the semi-analytical solutions and show the spatial variation of the potential, the instantaneous reflection and transmission coefficients and wave functions graphically by using WKB method for the two cases in physical region. We also use a quantum mechanical method to calculate the reflection coefficient numerically and compare the results by the two methods. In Section 5 we compare the results of different parameters. Finally in Section 6 we draw a conclusion.

We adopt the signature $(-\ +\ +\ +)$ and put $\hbar = G = C = 1$.

2. THE DIRAC EQUATION IN SdS GEOMETRY

The line element in SdS space takes the form

$$ds^2 = -\left(1 - \frac{2M}{r} - \frac{\Lambda}{3}r^2\right)dt^2 + \frac{dr^2}{1 - \frac{2M}{r} - \frac{\Lambda}{3}r^2} + r^2\,d\theta^2 + r^2\,\sin^2\theta d\varphi^2. \tag{1}$$

Following Chandrasekhar (1976, 1983), we obtained the Dirac equation in SdS geometry and separated it into radial and angular wave functions. The coupled

radial equations are given by

$$\Delta^{1/2} D_o R_{-1/2} = (\lambda + imr)\Delta^{1/2} R_{+1/2}, \tag{2a}$$

$$\Delta^{1/2} D_o^{\dagger} \Delta^{1/2} R_{+1/2} = (\lambda - imr) R_{-1/2}, \tag{2b}$$

and the angular equations can be written as

$$L_{1/2} S_{+1/2} = -\lambda S_{-1/2}, \tag{2c}$$

$$L_{1/2}^{\dagger} S_{-1/2} = -\lambda S_{+1/2}, \tag{2d}$$

where

$$D_n = \partial_r + \frac{ir^2\sigma}{\Delta} + 2n\frac{r - M - \frac{2}{3}\Lambda r^3}{\Delta}, \tag{3a}$$

$$D_n^{\dagger} = \partial_r - \frac{ir^2\sigma}{\Delta} + 2n\frac{r - M - \frac{2}{3}\Lambda r^3}{\Delta}, \tag{3b}$$

$$L_n = \partial_\theta + n\ \cot\theta + m\ cosec\,\theta, \tag{3c}$$

$$L_n^{\dagger} = \partial_\theta + n\ \cot\theta - m\ cosec\,\theta, \tag{3d}$$

$$\Delta \equiv r^2 - 2Mr - \frac{\Lambda}{3} r^4. \tag{3e}$$

Here n is an integer, σ is the frequency of incoming Dirac wave. M is the mass of the black hole, m is the rest mass of the Dirac particles, and $R_{\pm 1/2}$ are the radial wave functions corresponding to spin $\pm\frac{1}{2}$, $S_{\pm 1/2}$ are the angular functions. Δ is called horizon function.

The cosmological constant Λ is included in the horizon function. It only affects the radial parts of Dirac equation. The angular equations have the same form with that in Schwarzschild geometry. The eigenvalue of the angular equation for spin $\pm\frac{1}{2}$ is obtained as $\lambda = (\ell + \frac{1}{2})^2$ (Chakrabarti, 1984; Newman and Penrose, 1966; Goldberg *et al.*, 1967), where ℓ is the orbital quantum number and λ is the separation constant. Here, we choose $\ell = \frac{1}{2}$ and then $\lambda = 1$. We can explore the nature of the solutions for other orbital quantum numbers in future.

Following Chandrasekhar's approach, we easily reduce the coupled radial equations to one dimentional wave equations.

Define tortoise coordinate (Brevik and Simonsen, 2001)

$$r_* = \int \frac{dr}{f(r)}. \tag{4}$$

Here, $f(r) = 1 - \frac{2M}{r} - \frac{\Lambda}{3} r^2 = \frac{\Lambda}{3r}(r - r_e)(r - r_o)(r_c - r)$, where r_e is the event radius, r_c is the cosmological radius, and $r_o = -(r_e + r_c)$ which appears to be of

no physical significance. After defining surface gravities κ_i, the tortoise coordinate in SdS space takes the form

$$r_* = \frac{1}{2\kappa_e}\ln\left(\frac{r}{r_e}-1\right) - \frac{1}{2\kappa_c}\ln\left(1-\frac{r}{r_c}\right) + \frac{1}{2\kappa_o}\ln\left(1-\frac{r}{r_o}\right), \tag{5}$$

where

$$\kappa_e = \frac{(r_c-r_e)(r_e-r_o)}{6r_e}\Lambda, \tag{6a}$$

$$\kappa_c = \frac{(r_c-r_e)(r_c-r_o)}{6r_c}\Lambda, \tag{6b}$$

$$\kappa_o = \frac{(r_o-r_e)(r_c-r_o)}{6r_o}\Lambda, \tag{6c}$$

(for $r_e < r < r_c$)

$$\frac{d}{dr_*} = \frac{\Delta}{r^2}\frac{d}{dr}, \tag{7}$$

in terms of r_*, the operators take the forms

$$D_o = \frac{r^2}{\Delta}\left(\frac{d}{dr_*}+i\sigma\right) \quad \text{and} \quad D_o^\dagger = \frac{r^2}{\Delta}\left(\frac{d}{dr_*}-i\sigma\right). \tag{8}$$

Choosing $\Delta^{1/2}R_{+1/2} = P_{+1/2}$, $R_{-1/2} = P_{-1/2}$, Eqs. (2a) and (2b) become

$$\left(\frac{d}{dr_*}+i\sigma\right)P_{-1/2} = \frac{\Delta}{r^2}(1+imr)P_{+1/2}, \tag{9}$$

$$\left(\frac{d}{dr_*}-i\sigma\right)P_{+1/2} = \frac{\Delta}{r^2}(1-imr)P_{-1/2}, \tag{10}$$

We choose

$$\theta = \tan^{-1}(mr), \tag{11}$$

which yields $\cos\theta = 1/\sqrt{1+m^2r^2}$, $\sin\theta = mr/\sqrt{1+m^2r^2}$ and

$$(1 \pm imr) = e^{\pm i\theta}\sqrt{1+m^2r^2}. \tag{12}$$

Following exactly Chandrasekhar's approach we write

$$P_{+1/2} = \psi_{+1/2}\exp\left[-\frac{1}{2}i\,\tan^{-1}(mr)\right], \tag{13a}$$

$$P_{-1/2} = \psi_{-1/2}\exp\left[+\frac{1}{2}i\,\tan^{-1}(mr)\right], \tag{13b}$$

Finally, a choice of

$$\hat{r}_* = r_* + \frac{1}{2\sigma}\tan^{-1}(mr), \tag{14a}$$

yields

$$d\hat{r}_* = \left(1 + \frac{\Delta}{r^2}\frac{m}{2\sigma}\frac{1}{1+m^2r^2}\right)dr_*. \tag{14b}$$

With these definitions, the differential Eqs. (2a) and (2b) are re-written as

$$\left(\frac{d}{d\hat{r}_*} - i\sigma\right)\psi_{+1/2} = W\psi_{-1/2}, \tag{15a}$$

$$\left(\frac{d}{d\hat{r}_*} + i\sigma\right)\psi_{-1/2} = W\psi_{+1/2}, \tag{15b}$$

where

$$W = \frac{\Delta^{1/2}(1+m^2r^2)^{3/2}}{r^2(1+m^2r^2) + m\Delta/2\sigma}. \tag{16}$$

Let

$$Z_\pm = \psi_{+1/2} \pm \psi_{-1/2}, \tag{17}$$

we readily obtain a pair of one dimensional wave equations from the above equations

$$\left(\frac{d^2}{d\hat{r}_*^2} + \sigma^2\right)Z_\pm = V_\pm Z_\pm, \tag{18}$$

where

$$\begin{aligned} V_\pm &= W^2 \pm \frac{dW}{d\hat{r}_*} \\ &= \frac{\Delta^{1/2}(1+m^2r^2)^{3/2}}{[r^2(1+m^2r^2)+m\Delta/2\sigma]^2}\left[\Delta^{1/2}(1+m^2r^2)^{3/2}\right. \\ &\quad \left.\pm\left(\left(r - M - \frac{2}{3}\Lambda r^3\right)(1+m^2r^2) + 3m^2r\Delta\right)\right] \\ &\quad \mp \frac{\Delta^{3/2}(1+m^2r^2)^{5/2}}{[r^2(1+m^2r^2)+m\Delta/2\sigma]^3}\left[2r(1+m^2r^2)\right. \\ &\quad \left. + 2m^2r^3 + m\left(r - M - \frac{2}{3}\Lambda r^3\right)\Big/\sigma\right]. \end{aligned} \tag{19}$$

Equation (18) is nothing but one dimensional Schrödinger equation corresponding to the total energy of the wave σ^2 and potential energy $V_{\pm}$. It is clear that we obtain well behaved functions by using r_* (and $\hat{r}_*$) instead of r. The horizons are shifted to infinity. On the other hand, Eq. (18) is a non-linear equation, we couldn't give the analytical solution of it exactly. While in the limiting case when $\hat{r}_* \to \pm\infty$, $V \to 0$, the analytical solution can be given. Here we'll use a semi-classical method to draw the wave functions in the whole range of $\hat{r}_*$.

3. PARAMETER SPACE AND THE METHOD TO SOLVE EQUATIONS

Following the approach of Mukhopadhyay and Chakrabarti (1999, 2000), we choose the parameters in such a way that there is a significant interaction between the particle and the black hole. Then the Compton wavelength of the incoming wave is of the same order as SdS radius, i.e.

$$r_e \sim \frac{1}{m}. \tag{20}$$

Similarly, the frequency of the incoming particle will be of the same order as inverse of time. So

$$\frac{1}{r_e} \sim \sigma. \tag{21}$$

Then we obtain

$$m \sim \sigma \sim \frac{1}{r_e}. \tag{22}$$

It means we shall concentrate the region of parameter space close to $m = \sigma$, then the solution would be interesting as pointed out above.

We construct a parameter space in terms of m and σ. Figure 1(a) and (b) show the parameter spaces corresponding to two limiting cases separately. The first case is the Nariai case where we choose $\Lambda = 0.11$, the second case is when the two horizons are far apart, we choose $\Lambda = 0.001$ (Brevik and Simonsen, 2001). Note we have chosen M (mass of the black hole) $= 1$.

The parameter space includes physical space ($\sigma > m$) and unphysical space ($\sigma < m$). We solve the equation in physical space. This space is divided into two regions—I: $E > V_m$ and II: $E < V_m$, where E is equal to σ^2 and V_m is the maximum of the potential. We'll show the solutions in these two regions separately. From Fig. 1 we can see the boundary of region I and II in case of $\Lambda = 0.11$ is pushed to the left compared with that when $\Lambda = 0.001$. According to this, we can predict that when $0.001 < \Lambda < 0.11$, the boundary will be between the two boundaries in the above two limiting cases. Whatever be the value of Λ and the physical parameters, the energy of the incoming particle is always greater than the potential energy and WKB approximation is generally valid in the whole range in region I.

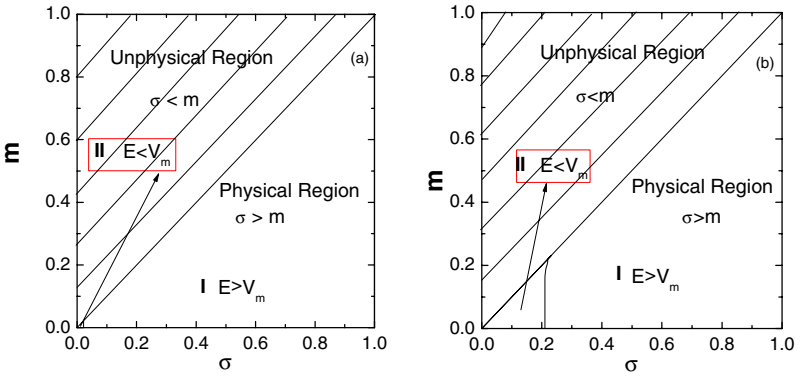

Fig. 1. Parameter space in terms of the energy and rest mass of the particles for (a) $\Lambda = 0.11$, (b) $\Lambda = 0.001$.

In region II, at two points total energy matches with the potential energy and in the neighbour of those two points WKB approximation is not valid. One has to employ different method such as Airy functions method to find solutions in this region.

4. SOLUTIONS OF DIRAC EQUATION

4.1. Solution of Region I

We rewrite Eq. (18) as

$$\frac{d^2 Z_+}{d\hat{r}_*^2} + (\sigma^2 - V_+)Z_+ = 0 \tag{23}$$

It can be solved by WKB approximation method because the energy of the incoming wave is always greater than the potential energy. In Fig. 2(a) and (b), we show contours of $\omega_{\max} = \max\left(\frac{1}{k^2}\frac{dk}{d\hat{r}_*}\right)$ for a given set (σ, m) of parameters for two limiting cases, where $k = \sqrt{\sigma^2 - V_+}$.

From Fig. 2(a) and (b), we can see WKB approximation is safely valid for any value of $\hat{r}_*$ except for parameters very close to the boundary of regions I and II. In Fig. 2a, the parameter space where WKB method being valid is much more broad than that in Fig. 2b. Let

$$u(\hat{r}_*) = \int k(\hat{r}_*)d\hat{r}_* + \text{conts.} \tag{24}$$

The solution of the Eq. (23) is

$$Z_+ = \frac{A_+}{\sqrt{k}}\exp(iu) + \frac{A_-}{\sqrt{k}}\exp(-iu), \tag{25}$$

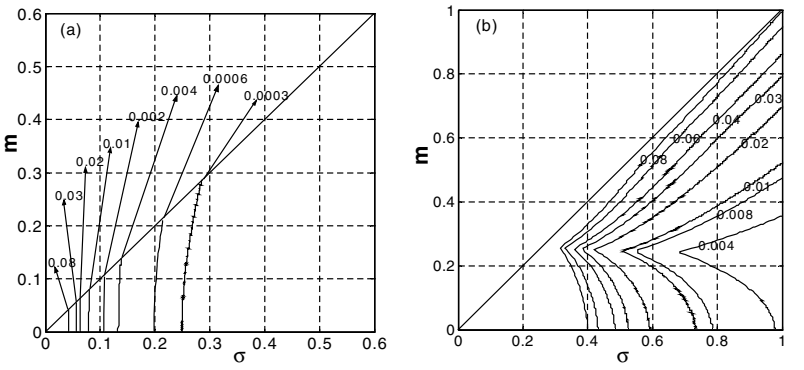

Fig. 2. Contours of constants $\omega_{\max} = \max(|\frac{l}{k^2}\frac{dk}{d\hat{r}_*}|)$ for (a) $\Lambda = 0.11$, (b) $\Lambda = 0.001$.

with

$$A_+^2 + A_-^2 = k. \tag{26}$$

$A_\pm$ are kept constants throughout in a standard WKB solution. But in our case the reflection coefficient on the inner horizon should be zero then $A_\pm$ are spatial dependent, so the standard WKB approximation requies a slight modification which will be shown later. While at a large distance far apart from the two horizons where WKB is strictly valid (this can be seen from the relation between $\frac{1}{k^2}\frac{dk}{d\hat{r}_*}$ and $\hat{r}_*$), A_+ and A_- should tend to be constants, then their difference is also a constant, i.e.

$$A_+ - A_- = c. \tag{27}$$

Here, c is a constant and is determined from the WKB solution at a large distance far apart from the two horizons. It with (26) gives

$$A_\pm(r) = \pm\frac{c}{2} + \frac{\sqrt{2k(r) - c^2}}{2}. \tag{28}$$

This relation can be not satisfied on the inner horizon. We introduce boundary condition: the refleced component vanishes on the inner boundary. Let A_{-h_e} be the values of A_- on the inner horizon, i.e.

$$A_{-h_e} = -\frac{c}{2} + \frac{\sqrt{2k(r_e) - c^2}}{2}. \tag{29a}$$

Similarly on the outer boundary

$$A_{-h_c} = -\frac{c}{2} + \frac{\sqrt{2k(r_c) - c^2}}{2}. \tag{29b}$$

Since $k(r_c) = k(r_e)$, we have $A_{-h_c} = A_{-h_e}$, that means the instantaneous reflecting situations are the same on the two horizons.

It is appropriate to use $\tilde{A}_- = (A_- - A_{-h_e})$ rather than A_- since $\tilde{A}$ vanishes at $r = r_e$. Similarly let $\tilde{A}_+ = (A_+ - A_{+he})$. Then one obtains physical R and T on the horizon.

With these conditions, the solution (25) becomes

$$Z_+ = \frac{\tilde{A}_+}{\sqrt{q}} \exp(iu) + \frac{\tilde{A}_-}{\sqrt{q}} \exp(-iu), \tag{30}$$

and

$$\tilde{A}_+^2 + \tilde{A}_-^2 = q. \tag{31}$$

Here, q is to be determined by equating the asymptotic behavior of this reflection coefficient with that obtained by using WKB method. The condition $|\frac{1}{q^2}\frac{dq}{d\hat{r}_*}| \ll 1$ is found to be satisfied whenever $|\frac{1}{k^2}\frac{dk}{d\hat{r}_*}| \ll 1$ is satisfied. Using the new notations, the instantaneous reflection and transmission coefficients are given by

$$R = \frac{\tilde{A}_-^2}{q}, \quad T = \frac{\tilde{A}_+^2}{q}. \tag{32}$$

We assume the normalization condition of $R + T = 1$. Similarly we can get Z_- corresponding potential V_- as

$$Z_- = \frac{\tilde{A}'_+}{\sqrt{q'}} \exp(iu') - \frac{\tilde{A}'_-}{\sqrt{q'}} \exp(-iu'), \tag{33}$$

the negative sign in front of the reflected wave is to satisfy the asymptotic property of the wave functions which must conserve the Wronskian (Chankrasekhar, 1983).

We should note that the reflection and transmission coefficients which are spatial dependence are the "local" or "instantaneous" values. The wave functions (30, 33) are valid in the whole space. So the WKB approximation used here should be called instantaneous WKB (IWKB for short). This name is first given in Mukhopadhyay and Chakrabarti (1999).

Using the solutions of equations with potential $V_\pm$ and the variations above, we obtain the radial wave functions $R_{+1/2}$ and $R_{-1/2}$ for spin up and spin down particles respectively of the original Dirac equation

$$R_e(R_{1/2}\Delta^{1/2}) = \frac{a_+ \cos(u - \theta) + a_- \cos(u + \theta)}{2\sqrt{k}} + \frac{a'_+ \cos(u' - \theta) - a'_- \cos(u' + \theta)}{2\sqrt{k'}}, \tag{34a}$$

$$I_m(R_{1/2}\Delta^{1/2}) = \frac{a_+\sin(u-\theta) - a_-\sin(u+\theta)}{2\sqrt{k}} + \frac{a'_+\sin(u'-\theta) + a'_-\sin(u'+\theta)}{2\sqrt{k'}}, \tag{34b}$$

$$R_e(R_{-1/2}) = \frac{a_+\cos(u+\theta) + a_-\cos(u-\theta)}{2\sqrt{k}} - \frac{a'_+\cos(u'+\theta) - a'_-\cos(u'-\theta)}{2\sqrt{k'}}, \tag{34c}$$

$$I_m(R_{-1/2}) = \frac{a_+\sin(u+\theta) - a_-\sin(u-\theta)}{2\sqrt{k}} - \frac{a'_+\sin(u'+\theta) + a'_-\sin(u'-\theta)}{2\sqrt{k'}}, \tag{34d}$$

where $a_+ = \frac{\tilde{A}_+}{\sqrt{q/k}}$, $a_- = \frac{\tilde{A}_-}{\sqrt{q/k}}$. $\frac{a'_+}{\sqrt{k'}}$ and $\frac{a'_-}{\sqrt{k'}}$ are the transmitted and reflected amplitudes respectively of the wave corresponding to potential V_-.

In Fig. 3(a) and (b), we show the nature of the potential for two cases. It is clear that potential $V_\pm$ are well behaved. They decrease as the particle approaches the two horizons. The maximum of the potential corresponding to $\Lambda = 0.001$ is much higher than that corresponding to $\Lambda = 0.11$. For concreteness, we solve the equations corresponding to potential V_+. In Fig. 4, the nature of V_+ (solid line), k (dashed line) and E (dotted line) for $\Lambda = 0.001$ are shown. As V_+ decreasing

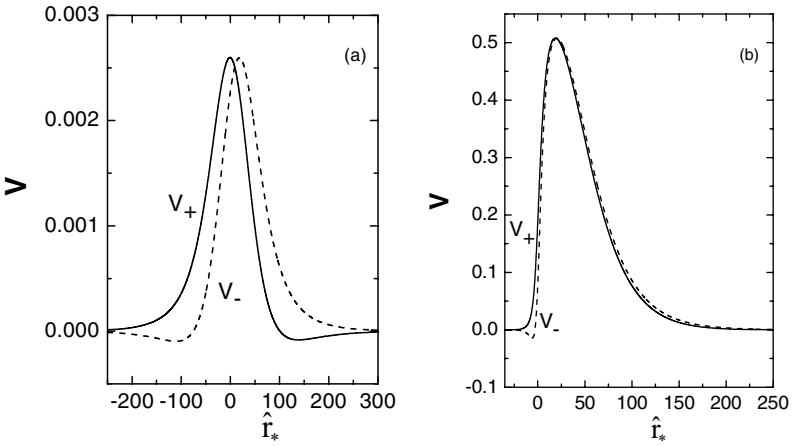

Fig. 3. Behaviour of V_+ (*solid*) and V_- (*dashed*) for (a) $\Lambda = 0.11$, (b) $\Lambda = 0.001$.

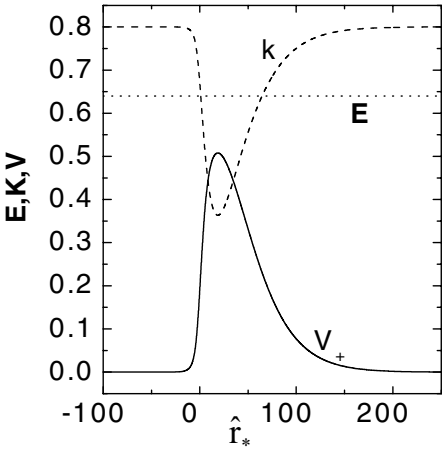

Fig. 4. $V_+(\hat{r}_*)$, $k(\hat{r}_*)$ and E for $\Lambda = 0.001$.

near the horizons k goes up. The picture of V_+, k and E for $\Lambda = 0.11$ is not given because V_+ is so low that the variation of k is not clear.

In Fig. 5(a) and (b) we show the variation of instantaneous reflection and transmission coefficients. The instantaneous reflection coefficients of the two limiting cases vanish on the two horizons. This can be understood because the local values of the reflection coefficient is only determined by the local potential from

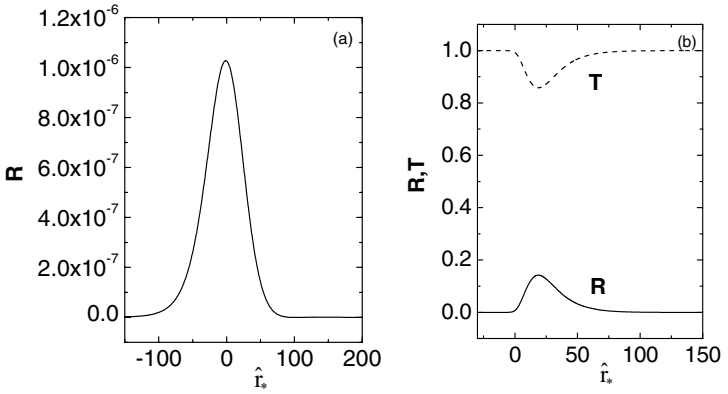

Fig. 5. (a) Instantaneous reflection (R) coefficienct for $\Lambda = 0.11$, (b) Instantaneous transmission (T) (*dotted*) and reflection (R) (*solid*) coefficiencts for $\Lambda = 0.001$.

Eq. (32) and the boundary condition. The potential energy turns out to be a constant (zero) on the two horizons, so the reflection coefficients on the two horizons have the same behavior, while we have assumed the zero value of the reflection on the inner boundary then the zero local value on the outer boundary is acceptable. On the other hand the value of the reflection coefficient for $\Lambda = 0.11$ is so small we only draw the instantaneous reflection coefficient for it and the instantaneous transmission coefficient would be $T = 1 - R$. Thus the larger the value of Λ the higher the maximum of the reflection coefficient. Then when $\Lambda = 0$, the maximum of the reflection coefficient should be the largest one for all non-negative Λ value. In Mukhopadhyay and Chakrabarti (1999) the Schwarzschild case is discussed, the result showed that the maximum of the reflection coifficient (about 0.7) is much higher than ours (about 0.14 for $\Lambda = 0.001$ and about 1.03×10^{-6} for $\Lambda = 0.11$ with the same set of parameters $\sigma = m = 0.8$).

We show the wave functions for $\Lambda = 0.11$ in Fig. 6(a–d) and $\Lambda = 0.001$ in Fig. 7(a–d). In each case, we give the function images for both the spin $+1/2$ and spin $-1/2$ particles respectively.

It is obvious that the amplitude as well as the wavelength of the wave functions remain constants when close to the two horizons where $V_{\pm}$ are constants. In case of $\Lambda = 0.11$, the wavelength is almost a constant in the whole range of $\hat{r}_*$ because there is very little variation of potential $V(\hat{r}_*)$. While when the two horizons are far apart from each other there is an obvious variation of the wavelength in the whole range. The wave length is prolonged by the potential barrier when the particle transmits toward the black hole. The amplitude of $R_e(\Delta^{1/2}R_{+1/2})$ and $Im(\Delta^{1/2}R_{+1/2})$ increases while the amplitude of $R_e(R_{-1/2})$ and $Im(R_{-1/2})$ decreases in the areas far away from the horizons. When $\Lambda = 0$, we get the figure of the wave functions in Schwarzschild geometry which was discussed in Mukhopadhyay and Chakrabarti (1999).

In fact, local values of the reflection and transmission coefficients could also be calculated numerically by using quantum mechanical approach. We only discuss the case of $\Lambda = 0.001$. First we replace the potentials (shown in Fig. 3(b)) by a collection of step functions as shown in Fig. 8(a)(only give the figure of V_+). In reality, we use as many as 10,000 steps to accurately follow the shape of the potential. The wave function on each step should have the form as

$$Z_{+,n} = A_n \exp[ik_n \hat{r}_{*,n}] + B_n \exp[-ik_n \hat{r}_{*,n}]. \tag{35}$$

The following standard junction conditions are included to ensure the function smooth

$$Z_{+,n} = Z_{+,n+1} \tag{36}$$

$$\left.\frac{dZ_+}{d\hat{r}_*}\right|_n = \left.\frac{dZ_+}{d\hat{r}_*}\right|_{n+1} \tag{37}$$

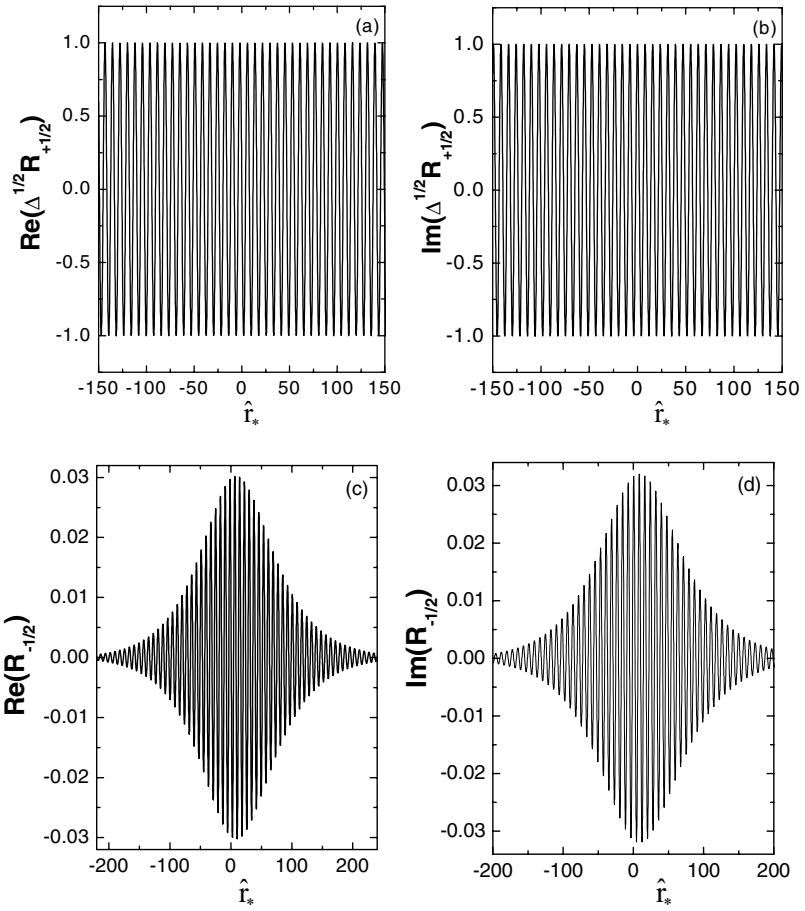

Fig. 6. Nature of real and imaginary parts of radial wave functions for $\Lambda = 0.11$.

The instantaneous reflection coefficient and the transmission coefficient have the forms $R_n = \frac{|B_n|^2}{|A_n|^2}$, $T_n = 1 - R_n$ respectively. To calculate the reflection and transmission coefficients at each junction, we also assume the inner boundary condition that the reflection coefficient vanishes when $r = r_e$. In Fig. 8(b) we show the instantaneous reflection coefficients obtained by the two methods. The two curves agree with each other perfectly which means the IWKB method is successfully valid intantaneously.

We have chosen $m = \sigma = 0.8$, $M = 1$ in all above calculations.

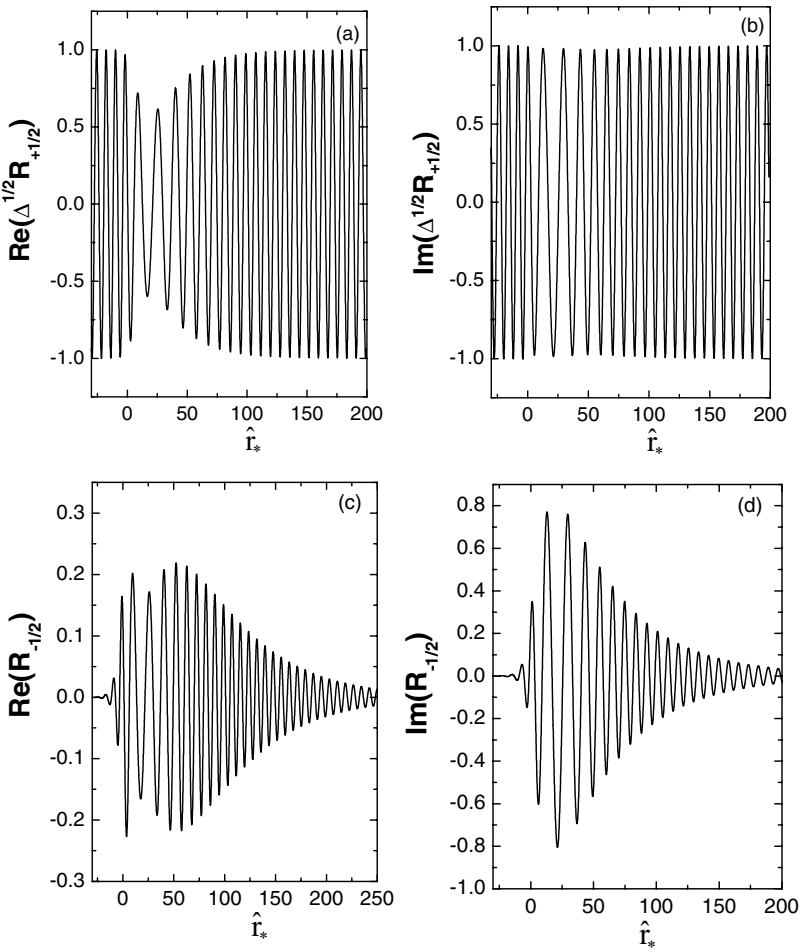

Fig. 7. Behaviour of radial wave functions for $\Lambda = 0.001$.

4.2. Solution of Region II

In this region, the total energy of the incoming particle is less than the maximum value of the potential. Then the WKB method is not valid in the whole range of $\hat{r}_*$. In the range except the neighbour of the two points at which total energy matches with the potential energy the WKB approximation is still valid. So the reflection and transmission coefficients and the wave function can be calculated in the same way described before. While when the potential energy dominates over the total energy, the solution will take the form $\frac{\exp(+u)}{\sqrt{k}}$ and $\frac{\exp(-u)}{\sqrt{k}}$. In the

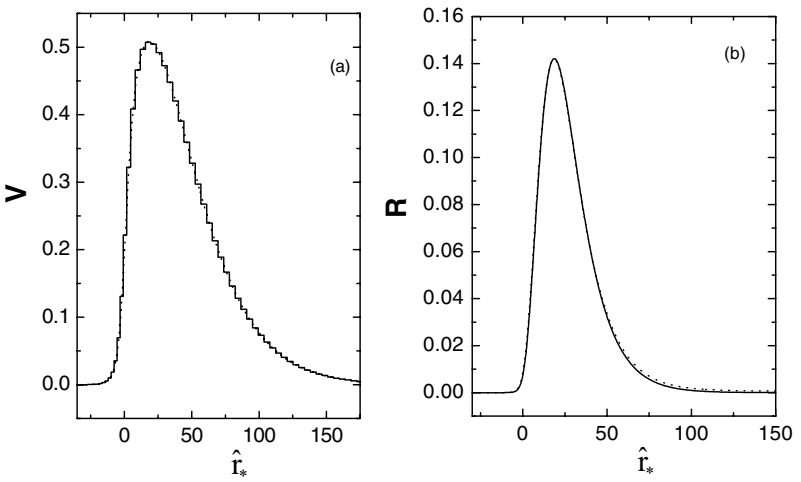

Fig. 8. (a) Step (*solid*) approximating a potential (*dotted*). (b) Comparison of variation of reflection coefficient R using WKB method (*solid*) and step-potential method (*dotted*).

range where WKB is not valid, the solution will be a linear combination of Airy functions because the potential is a approximately linear function of $\hat{r}_*$ in those intervals. The solutions with Airy founctions must match with that obtained by WKB approximation at the junctions. In the latter range, the equation reduces to

$$\frac{d^2 Z_+}{dx^2} - x Z_+ = 0, \tag{38}$$

where $x = \beta^{1/3}(\hat{r}_* - p)$, β is chosen to be positive and p is one of the turning points where the total energy matches with potential energy.

Let $Z_+(x) = x^{1/2} Y(x)$ and when $x > 0$ the Eq. (38) reduces to

$$x^2 \frac{d^2 Y}{dx^2} + x \frac{dY}{dx} - \left(x^3 + \frac{1}{4}\right) Y(x) = 0, \tag{39}$$

let $\xi = \frac{2}{3} x^{3/2}$, we obtain the modified Bessel equation

$$\xi^2 \frac{d^2 Y}{d\xi^2} + \xi \frac{dY}{d\xi} - \left(\xi^3 + \frac{1}{9}\right) Y(\xi) = 0, \tag{40}$$

the solution of which is $I_{+1/3}(\xi)$ and $I_{-1/3}(\xi)$. Hence the solution of Eq. (38) will be

$$Z_+(x) = x^{1/2}[C_1 I_{+1/3}(\xi) + C_2 I_{-1/3}(\xi)]. \tag{41}$$

Similarly we obtain the Bessel equation when $x < 0$

$$\xi^2 \frac{d^2Y}{d\xi^2} + \xi \frac{dY}{d\xi} + \left(\xi^2 - \frac{1}{9}\right) Y(\xi) = 0, \tag{42}$$

The corresponding solution is

$$Z_+(x) = |x|^{1/2}[D_1 J_{+1/3}(\xi) + D_2 J_{-1/3}(\xi)], \tag{43}$$

where $J_{\pm 1/3}$ and $I_{\pm 1/3}$ are the Bessel functions and the modified Bessel functions of order $\frac{1}{3}$ respectively.

The Airy functions are defined as

$$A_i(x) = \frac{1}{3} x^{1/2}[I_{-1/3}(\xi) - I_{+1/3}(\xi)], \quad x > 0, \tag{44a}$$

$$A_i(x) = \frac{1}{3} |x|^{1/2}[J_{-1/3}(\xi) + J_{+1/3}(\xi)], \quad x < 0, \tag{44b}$$

$$B_i(x) = \frac{1}{\sqrt{3}} x^{1/2}[I_{-1/3}(\xi) + I_{+1/3}(\xi)], \quad x > 0, \tag{44c}$$

$$B_i(x) = \frac{1}{\sqrt{3}} |x|^{1/2}[J_{-1/3}(\xi) - J_{+1/3}(\xi)], \quad x < 0. \tag{44d}$$

In terms of Airy functions, the solution (41)and (43) take the forms

$$Z_+ = \frac{3}{2}(C_2 - C_1) A_i(x) + \frac{\sqrt{3}}{2}(C_1 + C_2) B_i(x), \quad x > 0, \tag{45a}$$

$$Z_+ = \frac{3}{2}(D_2 + D_1) A_i(x) + \frac{\sqrt{3}}{2}(D_2 - D_1) B_i(x), \quad x < 0. \tag{45b}$$

In order to match boundary conditiaons $Z_+(+0) = Z_+(-0)$, we set $C_1 = -D_1$ and $C_2 = D_2$. Then the solution corresponding $x > 0$ and that corresponding $x < 0$ are continuous.

In Fig. 9(a) and (b) the nature of $V_\pm$ for the two cases are shown. The behavior is much like that in region I.

In Fig. 10(a) and (b) we show the nature of V_+ (*solid line*), k (*dashed line*) and energy E (*dotted line*). k^2 is negative in some region because σ^2 is no longer greater than $V_\pm$ at all radii.

For $\Lambda = 0.11$ case, in the region $\hat{r}_* \sim -125$ to -35 around the turning point $\hat{r}_* = -80.7352$, the solution turns out to be (Abramowitz and Stegun, 1966)

$$Z_+ = 1.560064\, A_i(x) + 0.721624\, B_i(x). \tag{46}$$

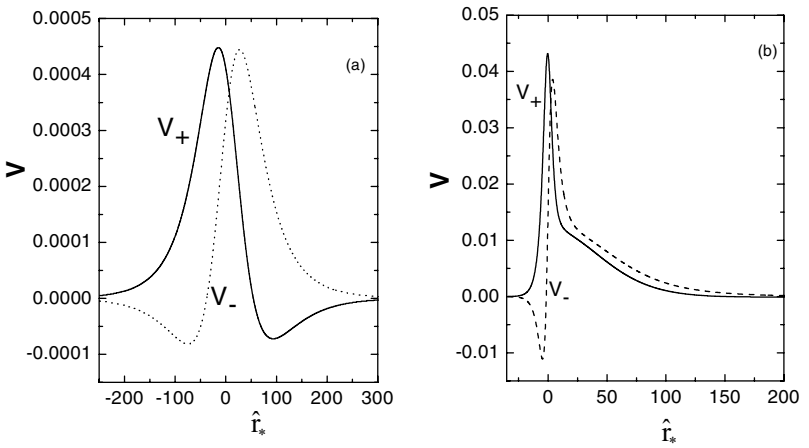

Fig. 9. Potential for (a) $\Lambda = 0.11$, (b) $\Lambda = 0.001$.

Similarly, the solution from $\hat{r}_* \sim -5$ to 65 around the other turning point $\hat{r}_* = 29.7591$ can be calculated as (Abramowitz and Stegun, 1966)

$$Z_+ = 1.574231\, A_i(x) + 0.714739\, B_i(x). \tag{47}$$

For $\Lambda = 0.001$, in the region $\hat{r}_* \sim -10$ to -2 around the turning point $\hat{r}_* = -5.9733$, the solution turns out to be (Abramowitz and Stegun, 1966)

$$Z_+ = 1.544757\, A_i(x) + 0.734712\, B_i(x), \tag{48}$$

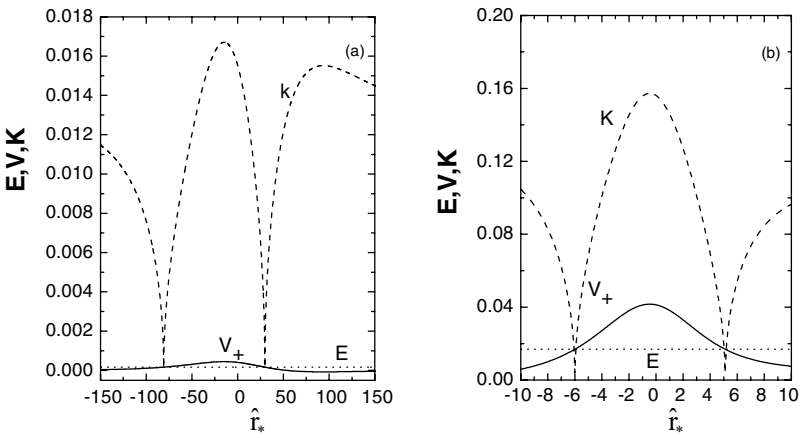

Fig. 10. Behaviour of k (*dashed*), V_+ (*solid*), E (*dotted*) for (a) $\Lambda = 0.11$, (b) $\Lambda = 0.001$.

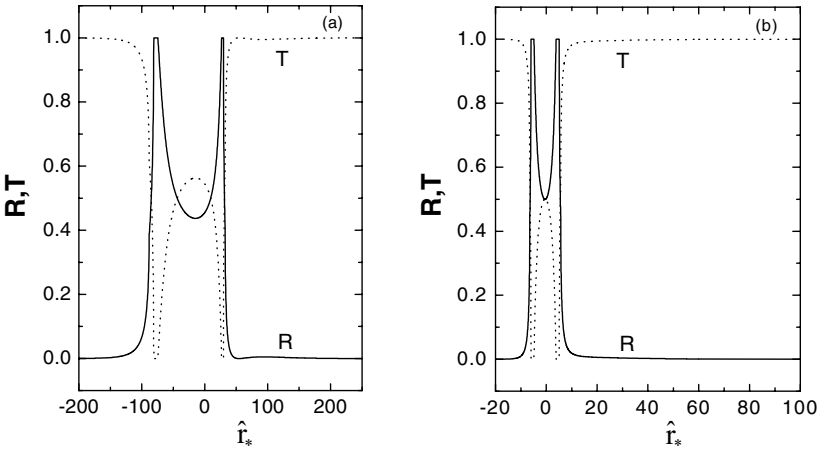

Fig. 11. R (*solid*) and T (*dotted*) for (a) $\Lambda = 0.11$, (b) $\Lambda = 0.001$.

the other turning point is $\hat{r}_* = 5.1163$, the solution in the region $\hat{r}_* \sim 1$ to 9 is

$$Z_+ = 1.471905\, A_i(x) + 0.767276\, B_i(x). \tag{49}$$

Note that the solutions with Airy functions match with that obtained by WKB approximation at the junctions.

In Fig. 11(a) and (b), we show the behaviors of reflection and transmission coefficients. The constants A_{-h_e} and A_{+h_e} are calculated as before.

We have chosen $M = 1, \sigma = 0.013, m = 0.009$ for $\Lambda = 0.11$ and $\sigma = 0.13$, $m = 0.07$ for $\Lambda = 0.001$ in all the calculations in this region.

5. SOLUTIONS OF DIFFERENT PARAMETERS

Black hole scatters incoming waves of different masses and different energies quite differently. Maybe black hole is a mass spectrograph (Mukhopadhyay and Chakrabarti, 1999, 2000). In this section we show a collection of solutions for the case of $\Lambda = 0.001$. In Fig. 12a we show the reflection and transmission coefficients for waves with parameters $\sigma = 0.8$ (*solid*), 0.9 (*dotted*), 0.98 (*dashed*) and $m = 0.8$. We can see the higher the particle's energy the larger the value of the transmission coefficient and the smaller the value of the reflection coefficient. In Fig. 12b the real part of the wave Z_+ corresponding to the three cases are shown. Near the two horizons the wave pattern is independent of σ. In order to show the difference of Z_+ for the three cases clearly we only plot the curves in a small range of $\hat{r}_*$. At a large distance except for the two horizons, the dispersal of the waves with different σ is clear. The smaller the energy of the particle the larger

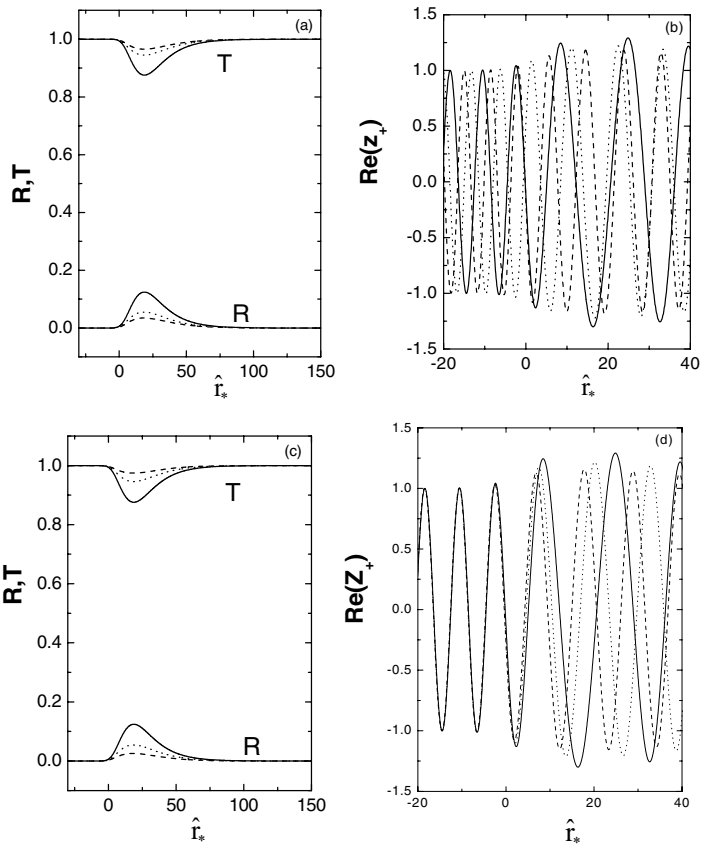

Fig. 12. Comparison of (a) R and T (b) real amplitude of the wave function Z_+ for $m = 0.8$ and $\sigma = 0.8$ (*solid*), 0.9 (*dotted*) and 0.98 (*dashed*) respectively. (c and d) Similar quantities for $\sigma = 0.8$ and $m = 0.8$ (*solid*), 0.72 (*dotted*) and 0.64 (*dashed*) respectively.

the wavelength and the higher the amplitude of $R_e(Z_+)$. In Fig. 12c we show the reflection and transmission coefficients for waves with parameters $m = 0.8$ (*solid*), 0.72 (*dotted*) and 0.64 (*dashed*) respectively while keeping $\sigma = 0.8$. In Fig. 12d the corresponding wave functions are shown. Close to the horizons the nature of the wave as well as the reflection and transmission coefficients are quite indepent of the rest mass of the partice. As the mass of the particle rises, the reflection goes up and the transmission goes down with the amplitude of $R_e(Z_+)$ goes up.

We don't show the solutions of different parameters for $\Lambda = 0.11$ because the potential is so low that the variation of reflection and transmission coefficients and wave functions for different parameters is much less pronounced than that for $\Lambda = 0.001$. We can predict as Λ dicreases the difference of results between different parameters is more and more obvious. When $\Lambda = 0$, it becomes the case of Schwarzschild black hole.

The particles with different masses and different energies can be dispersed clearly after being scattered by black hole. Black hole may act as a huge mass spectrograph.

6. SUMMARY

In this paper, we studied the scattering of Dirac particles in Schwarschild-de Sitter geometry by using WKB method. We gave the semi-analytical solution of Dirac equation and presented the nature of the instantaneous reflection and transmission coefficients and the radial wave functions for two limiting cases respectively.

We first classfied an entire parameter space in terms of the physical and unphysical region. The physical region was further divided into two parts depending on the height of potential and energy of the particle. In each region, we studied the two limiting cases. The first case is the two horizons are close to each other, we choose $\Lambda = 0.11$. The second case is when the two horizons are far apart, we choose $\Lambda = 0.001$. From the discussion on the two cases, we can predict the results for any case in this geometry when $0.001 < \Lambda < 0.11$. When $\Lambda = 0$, the result turned out to be that in Schwarzschild background which is studied in Mukhopadhyay and Chakrabarti (1999). We chose a group of parameters as example to study the nature of wave functions in each of the regions. From Fig. 2(a) and (b) we can obtain the regions where the WKB method is valid. In the regions where WKB solutions cannot be trusted, other methods such as Airy functions approach must be employed.

The standard WKB solution can not be accurate in the whole range, it required a slight modification. We gave the inner boundary condition, then the constants A_+ and A_- became spatial dependent and the solution was satisfying in the whole range. The reflection and transmission coefficients are all instantaneous values, they are defined at a single point, the significance of the instantaneous reflection and the transmission coefficients has been detailedly discussed in Mukhopadhyay and Chakrabarti (1999, 2000). So the WKB method used here was also called "instantaneous WKB" (IWKB for short) named by Mukhopadhyay and Chakrabarti (1999, 2000). Moreover, we use the step-potential method to solve the equation. The results getting from the two methods turned out to be agreed. So the IWKB method is valid.

Black hole can act as a huge mass spectrograph because it scatters waves with different parameters quite differently. This can be seen from Fig. 12(a–d). While when $\Lambda = 0.11$, the two horizons are so close to each other that the maximum of the potential barrier is much lower and the variation of the potential barrier is not clear whatever be the value of the parameters. Thus, the differentiation of transmission and reflection coefficients or waves with different parameters is much less pronounced than that when $\Lambda = 0.001$. In a way, a mixture of waves should be splitted into its components by the black hole as long as Λ is quite small.

The effect on the solutions by the cosmological constant can be not negligible from this paper, so the problem studied in this paper is significative if Λ is really present. On the other hand we can use this method and the corresponding results to discuss the problem of Hawking radiation in further.

REFERENCES

Abramowitz, M. and Stegun, I. A. (1966). *Handbook of Mathematical Functions with Formulas, Graphs, and Mathematical Tables* (Washington, National Bureau of Standards).
Brevik, I. and Simonsen, B. (2001). *General Relativity and Gravitation* **33**, 1839.
Chakrabarti, S. K. (1984). *Proceedings of Royal Society of London A* **391**, 27.
Chandrasekhar, S. (1976). *Proceedings of the Royal Society of London A* **349**, 571.
Chankrasekhar, S. (1983). *The Mathematical Theory of Black Holes* (New York, Oxford University Press).
Goldberg, J. N., *et al*. (1967). *Journal of Mathematical Physics* **8**, 2155.
Khanal, U. (1984). *Physics Review D* **32**, 879.
Khanal, U. and Panchapakesan, N. (1980). *Physics Review D* **24**, 829.
Kinnersley, W. (1969). *Journal of Mathematical Physics* **10**, 1195.
Liu, L. *et al*. (1980). *Acta Physica Sinica* **29**, 1617.
Mukhopadhyay, B. and Chakrabarti, S. K. (1999). *Classification of Quantum and Gravity* **16**, 3165.
Mukhopadhyay, B. and Chakrabarti, S. K. (2000). *Nuclear Physics B* **582**, 627.
Newman, E. and Penrose, R. (1966). *Journal of Mathematical Physics* **7**, 863.
Page, D. N. (1976). *Physics Review D* **14**, 1509.
Teukolsky, S. A. (1973). *Astrophysics Journal* **185**, 635.
Zhao, Z., Gui, Y. X., and Liu, L. (1981). *Acta Astrophysical Sinica* **1**, 141.